Scientific Research Publishing

Geomaterials, 2026, 16(1), 1-18
https://www.scirp.org/journal/gm
ISSN Online: 2161-7546
ISSN Print: 2161-7538

Modeling the Shrinkage-Swelling of Clay Soils of Diamniadio Using the Method Based on the Module of Elasticity (Mebm)

Khadim Faye, Fatou Samb, Pape Sanou Faye, Yves Berthaud

Laboratoire de Mécanique et Modélisation, UFR Sciences de l'Ingénieur, UIDT, Thiès, Sénégal
Email: fayebamba2014@gmail.com

How to cite this paper: Faye, K., Samb, F., Faye, P.S. and Berthaud, Y. (2026) Modeling the Shrinkage-Swelling of Clay Soils of Diamniadio Using the Method Based on the Module of Elasticity (Mebm). *Geomaterials*, **16**, 1-18.
https://doi.org/10.4236/gm.2026.161001

Received: August 22, 2025
Accepted: December 9, 2025
Published: December 12, 2025

Abstract

The work presented in this article relating to the study of the behavior of swelling soils of Diamniadio has set itself the objective of modeling the shrinkage-swelling of crumb marl, foliated at-tapulgite marl and sandy clay. to limestone concretion using the method based on the elastic modulus (MEBM) presented by Adam and Vanapolli (2013) [1]. This method, which focuses on soil-atmosphere interaction, makes it possible to predict changes in soil volume as a function of climate variation. In this study, soil swelling shrinkages were well estimated taking into account the associated suction and elastic modulus as key parameters. The latter are used in a constitutive relation for the change in volume which is based on the mechanics of unsaturated soils developed by Fredlund and Morgenstern (1976) [2]. This method is based on the two-dimensional software (VADOSE/W) which uses climatic data, the soil profile and their physical and geotechnical characteristics to determine variations in suction, an essential parameter for calculating vertical movements of the soil in the time.

Keywords

Swelling Clay, Expansive Soil, MEBM, Suction Shrinkage-Swelling, Elastic Modulus, Diamniadio

1. Introduction

Few studies in recent years have proposed procedures to estimate *in-situ* movements of expansive soils over time (Briaud *et al.*, 2003 [3]; Chao *et al.*, 2007 [4]; Vu *et al.* Fredlund, 2004 [5]; Zhang and Briaud, 2010) [6]. However, there are prediction methods that can be used in current practice to estimate volume change move-

ments in relation to environmental changes that are simple and economical. In the same vein, this study is devoted to the modeling of the vertical movements of the three swelling soils of the urban center of Diamniadio by the method based on the elastic modulus (MEBM) of which the different stages of the modeling will be detailed in the following. The work consists of making a prediction of the volume changes of the three soil types with a respective thickness of three meters over a period of fourteen months using climatic data from the national agency of civil aviation and meteorology of Senegal (ANACIM) 2020 [7]. In this article, we will first focus on determining the results from soil-atmosphere interaction using the VADOSE/W software, then we will proceed with modeling the shrink-swell behavior of these three types of soil using the method based on the modulus of elasticity (MEBM). To conclude, a comparison of the volumetric changes recorded by crumbly marl, laminated marl, and sandy clay during this period will be carried out.

2. Soil-Atmosphere Interaction

2.1. Climatique Data

Climate data for the last ten years were provided to us by the National Civil Aviation and Meteorology Agency (ANACIM, 2020). This data includes dominant wind direction, average wind speed (m/s), insolation in hours, cumulative rainfall in mm, average maximum and minimum temperature in degrees Celsius, maximum humidity in %, minimum humidity in %, and evaporation in mm. These values constitute input data in the VADOSE/W program at the level of the window representing the climatic parameters (see Table 1).

Table 1. The climatic parameters used in the modeling.

Months	Temperature °C		RH (%)		Wind	Precip	Precip	Priod	Evap./Trans.
	Max	Min	Max	Min	(m/s)	(mm)	Start	End (hr)	(mm/day)
November	34.4	23.3	91.5	48.1	3.6	22.6	0.0	24.0	4.2
December	35.6	20.4	69.0	25.3	4.4	0.0	0.0	24.0	8.4
January	34.4	18.3	70.3	15.2	4.3	0.0	0.0	24.0	7.8
February	33.5	18.3	57.2	11.6	4.6	0.0	0.0	24.0	12.0
March	37.0	21.0	59.6	14.4	4.8	0.0	0.0	24.0	13.0
April	36.1	20.4	76.2	23.0	5.1	0.0	0.0	24.0	11.0
May	34.2	20.1	79.2	31.1	5.4	0.0	0.0	24.0	9.4

After modeling the soil-atmosphere interaction over time, several parameters can be collected, such as the degree of saturation, suction, water content, infiltration, etc. In this study, we will model soil movements for a period of fourteen months, *i.e.* from November 2019 to December 2020. Regarding the monthly precipitation

measured in the study area during the period between November 2019 and December 2020, we see that the majority of rainfall occurred between June, July, August, September and October 2020 with a maximum of 206.3 mm/m^2 in September (see Figure 1). Regarding infiltration, we note that the negative values are between December 2019 and June 2020 with a maximum of −12.99 mm/m^2 in February 2020. In this interval, values are recorded very high suction. The evolution of the curve in Figure 2 shows that the month of June 2020 marks the start of the infiltration which reaches its maximum in the month of July (50.45 mm/m^2). Figure 3 allows us to make the correlation between rainfall, infiltration and radiation over the fourteen months. In this curve, we see that precipitation and infiltration evolve in the same direction while radiation partly governs evaporation.

We also note that the months of February, March, April, May and June record the greatest drying times. During this period, the soils will be subjected to intense evaporation phenomena leading to desiccation cracks in the surface areas and significant settlements which can cause cracks in the supported structures.

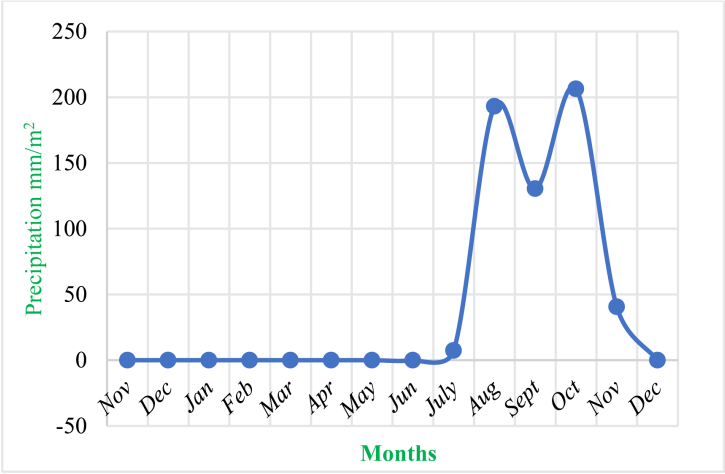

Figure 1. Precipitation variation curve for the last fourteen months.

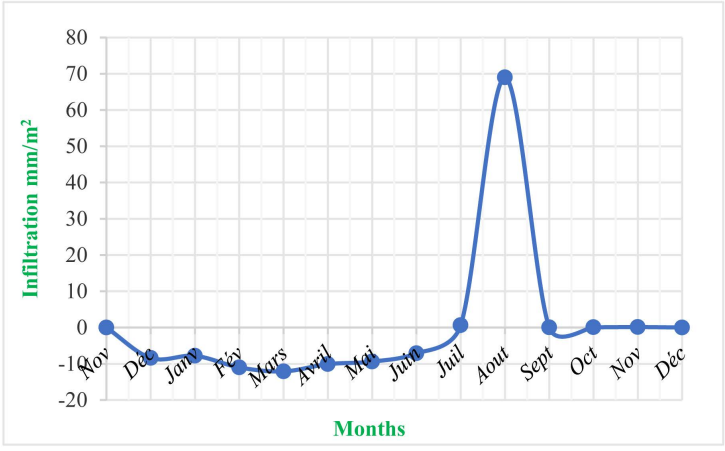

Figure 2. Infiltration curve.

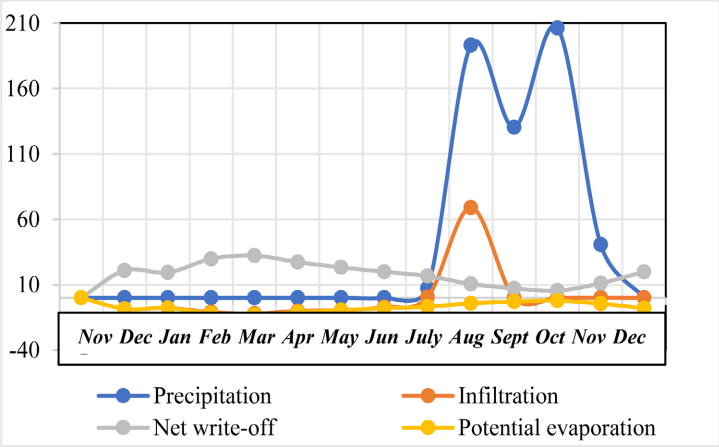

Figure 3. Correlation between rainfall, infiltration and solar radiation.

2.2. The Modeling Steps

The different stages of modeling soil volume variations using MEBM are grouped into three main stages:

- ✓ Laboratory tests which consist of determining the geotechnical and physical characteristics of the soil, namely the natural water content, the elastic modulus in the saturated state E_{sat} from the oedometric test as well as the water content. water in the saturated state w_{sat}, the void index in the natural state e_0 and the porosity n. The permeability k is determined from the variable volume permeability test and finally for what concerns the thermal conductivity, we took the theoretical value of these soils.
- ✓ Modeling with the VADOSE/W software of soil-atmosphere interaction which makes it possible to determine the variation in suction from climatic data and soil characteristics already determined in laboratory tests. In fact, the suction data comes from the soil-water characterization curve after projection of the volumetric water content values.
- ✓ The determination of ground movements by MEBM is obtained using the general volume variation equation $d\varepsilon_v = \frac{\Delta V_v}{V_0} = m_1^s d(\sigma - u_a) + m_2^s d(u_a - u_w)$, but before that preliminary calculations will be carried out to determine the modulus of elasticity in the unsaturated state E_{unsat}, the coefficient of total change with respect to changes in suction m_2^s, the modulus of elasticity with respect to change in suction H.

Figure 4 shows the different stages of the modeling.

3. Modeling of Soil Volume Change

3.1. Modeling of the Shrinkage and Swelling of the Crumbly Marl

For the soil parameters, we will need the saturated modulus of elasticity, dry density, porosity, solid grain density, permeability, thermal conductivity and degree of saturation. The values of these parameters are grouped in Table 2.

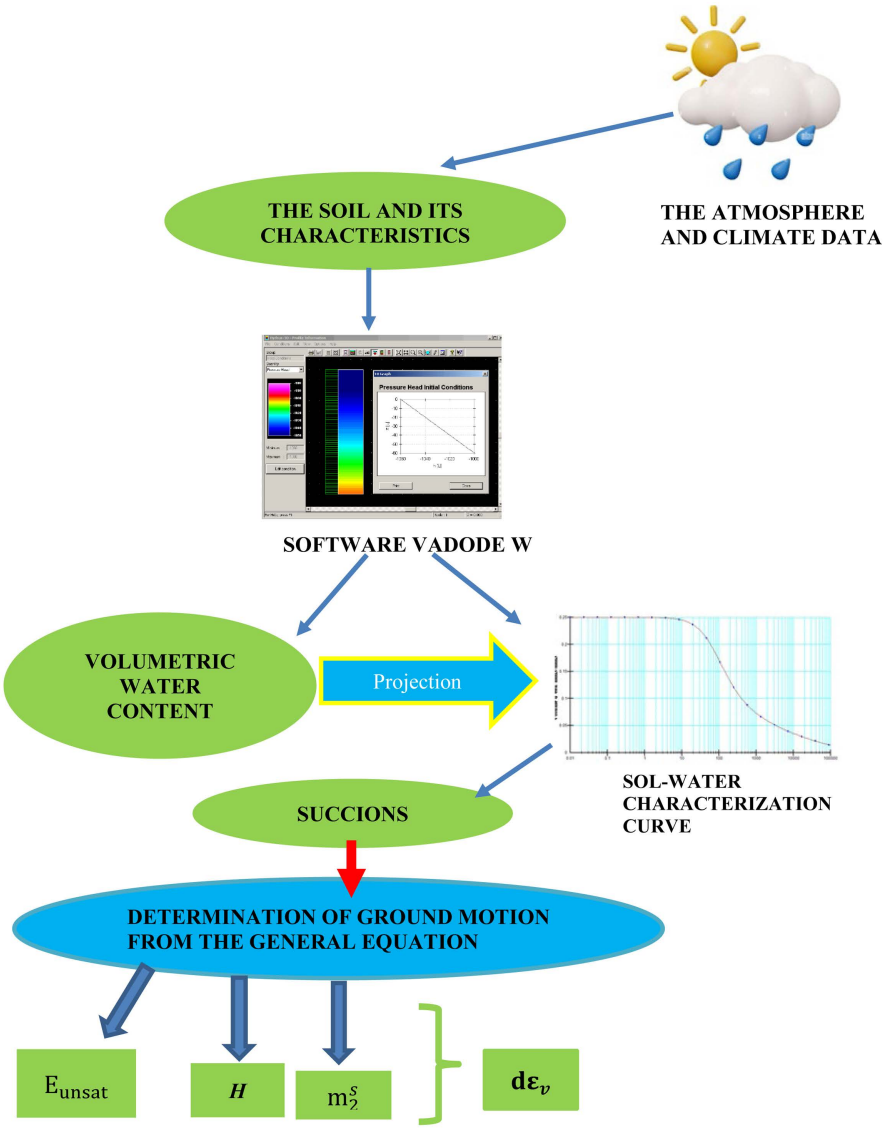

Figure 4. The different stages of modeling.

Table 2. Characteristics of marl.

Modulus of elasticity E kPa	Natural water content %	Saturated water content %	Void indive e_0	Porosity n	Permeability k (m/s)	Thermal conductivity (W/m/K)
8679.81	9.8	39.0	0.66	0.39	1.15E−09	2100

Figure 5 shows the profile of the crumbly marl, the surface layer, and the climatic conditions.

The strain variable associated with volume change was rationally interpreted in terms of two independent variables of the stress state of unsaturated soils, namely, matric suction $(u_a - u_w)$ and net normal stress $(\sigma - u_a)$ (Fredlund and Morgenstern, 1976).

$$d\varepsilon_v = \frac{\Delta V_v}{V_0} = m_1^s d\left(\sigma - u_a\right) + m_2^s d\left(u_a - u_w\right) \quad (1)$$

with m_1^s coefficient of volume variation linked to the net stress, m_2^s coefficient of volume variation linked to the matric suction $\left(\sigma - u_a\right)$, the net normal stress $\left(u_a - u_w\right)$ is the matric suction and d the thickness of the layer.

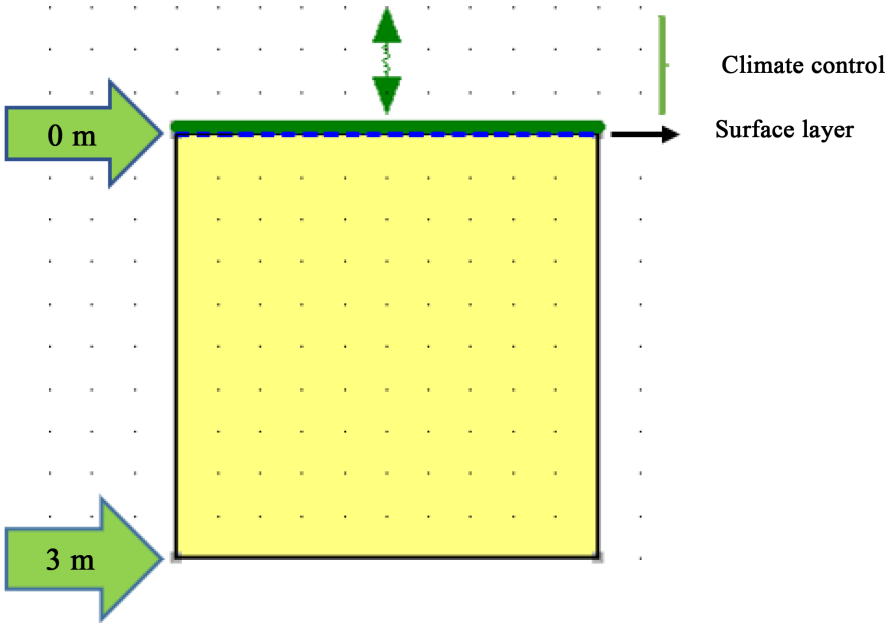

Figure 5. Profile of the crumbly marl.

The constitutive volume change relationship (Equation (1)) can be presented graphically as a three-dimensional constitutive surface (Figure 6).

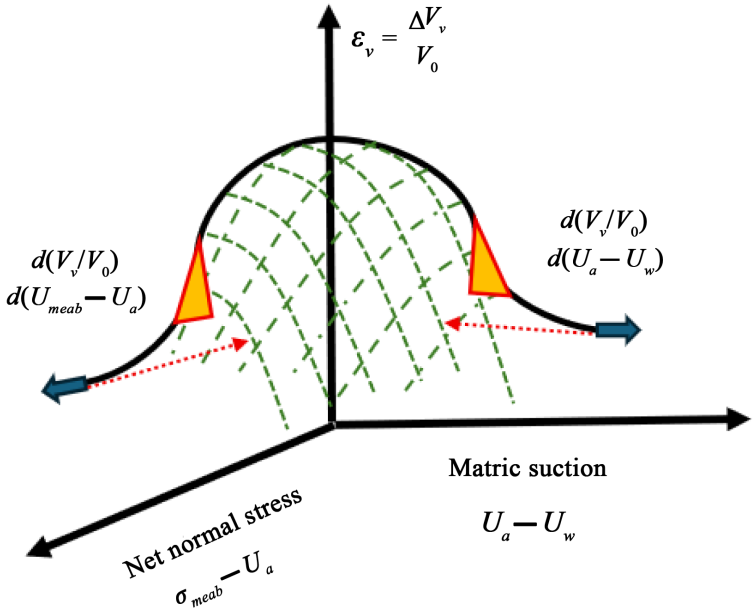

Figure 6. The constituent surface of the soil (modified after Fredlund et Rahardjo, 1993) [8].

However, for lightly loaded pavements and structures, the influence of mechanical stress (*i.e.* net normal stress) is not significant and can be neglected (Fredlund *et al*., 1980) [9]. In this case, only the change in matric suction will mainly contribute to the change in soil volume; Equation 1 reduces to Equation (2) as shown below.

$$d\varepsilon_v = m_2^s d\left(u_a - u_w\right) \tag{2}$$

In the first steps, we first determine the Volumetric Water Content which describes the volume of water a material can store based on the pore water pressure. These values are automatically generated by the software after entering climatic data and soil characteristics. These values vary with time and depth. The corresponding suctions are then determined from the soil-water characteristic curve (SWCC) in Figure 7.

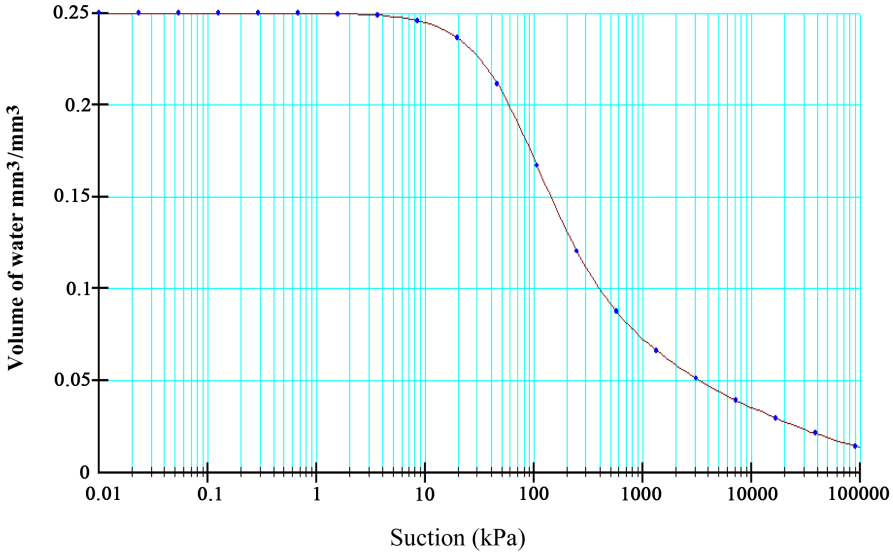

Figure 7. Soil-water characterization curve.

In the general equation (Equation (2)), the coefficient of total volume change with respect to suction changes m_2^s is determined from the elastic modulus with respect to suction change H by the following formula.

$$m_2^s = \frac{1+\nu}{H\left(1-\nu\right)} \tag{3}$$

The modulus of elasticity H is obtained using the modulus of elasticity in the unsaturated state according to Equation (4).

$$H = E_{un}/\left(1-2\nu\right) \tag{4}$$

with E_{un} the modulus of elasticity in the unsaturated state taken from the modulus of elasticity in the saturated state according to Equation (5).

$$E_{unsat} = E_{sat}\left[1+\alpha\frac{u_a-u_w}{\left(\frac{p_a}{101.3}\right)}s^{\beta}\right] \tag{5}$$

In modeling for each given water content, we will have to determine from the equations above the modulus of elasticity in the unsaturated state E_{unsat}, the coefficient of change in total volume with respect to changes in suction m_2^s and finally the vertical movement of the ground dh_i.

For the three meters thick of the crumb marl, we will arbitrarily take a few depths of which we will determine according to climatic variations over time their volumetric water contents, their suctions and their recorded vertical movements. Table 3 gives the different values of volumetric water content as a function of time and depth.

Table 3. Variation in the volume of water contained (m^3/m^3) over the last twelve months.

Depth (m)	Nov.	Dec.	Jan.	Feb.	March	Apr.	May
0	3.80E−01	3.00E−01	2.30E−01	2.20E−01	2.20E−01	2.30E−01	2.40E−01
0.5	3.80E−01	3.40E−01	3.00E−01	3.00E−01	3.00E−01	3.00E−01	3.10E−01
1	3.80E−01	3.80E−01	3.80E−01	3.80E−01	3.80E−01	3.80E−01	3.80E−01
1.5	3.90E−01	3.90E−01	3.90E−01	3.90E−01	3.90E−01	3.90E−01	3.90E−01
2	3.90E−01	3.90E−01	3.90E−01	3.90E−01	3.90E−01	3.90E−01	3.90E−01
2.5	3.90E−01	3.90E−01	3.90E−01	3.90E−01	3.90E−01	3.90E−01	3.90E−01
3	3.90E−01	3.90E−01	3.90E−01	3.90E−01	3.90E−01	3.90E−01	3.90E−01
Depth (m)	**Jun.**	**Jul.**	**Aug.**	**Sept.**	**Oct.**	**Nov.**	**Dec.**
0	2.50E−01	2.50E−01	2.60E−01	2.60E−01	2.60E−01	2.70E−01	2.70E−01
0.5	3.10E−01	3.20E−01	3.20E−01	3.20E−01	3.20E−01	3.30E−01	3.30E−01
1	3.80E−01	3.80E−01	3.80E−01	3.80E−01	3.80E−01	3.80E−01	3.80E−01
1.5	3.90E−01	3.90E−01	3.90E−01	3.90E−01	3.90E−01	3.90E−01	3.90E−01
2	3.90E−01	3.90E−01	3.90E−01	3.90E−01	3.90E−01	3.90E−01	3.90E−01
2.5	3.90E−01	3.90E−01	3.90E−01	3.90E−01	3.90E−01	3.90E−01	3.90E−01
3	3.90E−01	3.90E−01	3.90E−01	3.90E−01	3.90E−01	3.90E−01	3.90E−01

Depending on these variations in water volume, the corresponding suctions are determined in Table 4 from the soil-water characterization curve (see Figure 7).

Table 4. The variations in suction power as a function of depth and time.

Depth (m)	Nov.	Dec.	Jan.	Feb.	March	Apr.	May
0	8.50E+00	7.00E+01	1.50E+02	1.65E+02	1.65E+02	1.50E+02	1.40E+02
0.5	8.50E+00	3.80E+01	7.00E+01	7.00E+01	7.00E+01	7.00E+01	6.00E+01
1	8.50E+00	8.50E+00	8.50E+00	8.50E+00	8.50E+00	8.50E+00	8.50E+00

Continued

1.5	1.00E−02	1.00E−02	1.00E−02	1.00E−02	1.00E−02	1.00E−02	1.00E−02
2	1.00E−02	1.00E−02	1.00E−02	1.00E−02	1.00E−02	1.00E−02	1.00E−02
2.5	1.00E−02	1.00E−02	1.00E−02	1.00E−02	1.00E−02	1.00E−02	1.00E−02
3	1.00E−02	1.00E−02	1.00E−02	1.00E−02	1.00E−02	1.00E−02	1.00E−02
Depth (cm)	**Jun.**	**Jul.**	**Aug.**	**Sept.**	**Oct.**	**Nov.**	**Dec.**
0	1.20E+02	1.20E+02	1.06E+02	1.06E+02	1.06E+02	8.00E+01	8.00E+01
0.5	6.00E+01	5.00E+01	5.00E+01	5.00E+01	5.00E+01	4.57E+01	4.57E+01
1	8.50E+00	8.50E+00	8.50E+00	8.50E+00	8.50E+00	8.50E+00	8.50E+00
1.5	1.00E−02	1.00E−02	1.00E−02	1.00E−02	1.00E−02	1.00E−02	1.00E−02
2	1.00E−02	1.00E−02	1.00E−02	1.00E−02	1.00E−02	1.00E−02	1.00E−02
2.5	1.00E−02	1.00E−02	1.00E−02	1.00E−02	1.00E−02	1.00E−02	1.00E−02
3	1.00E−02	1.00E−02	1.00E−02	1.00E−02	1.00E−02	1.00E−02	1.00E−02

From these data, the ground displacements can be calculated at each depth from Equation (2). The values of the two parameters of the model, namely the coefficient α, are taken equal to 1/14 and β to 2.

The value $\beta = 2$ is used for expansive soils regardless of the value of the plasticity index Ip. The parameter was assumed to be (1/14) in order to provide reasonable shrink-swell prediction values.

The results reveal that the suction variations are higher in the superficial part. In the lower parts, the values gradually decrease. Subsequently, the vertical movements of the crumb marl with a thickness of three meters are calculated and grouped in Table 5.

Table 5. The swelling and shrinking of crumbly marl depending on climate variations and depth.

Depth (m)	Nov.	Dec.	Jan.	Feb.	March	Apr.	May
0	1.96E−03	1.54E−02	3.27E−02	3.58E−02	3.58E−02	3.27E−02	3.04E−02
0.5	1.96E−03	8.50E−03	1.54E−02	1.54E−02	1.54E−02	1.54E−02	1.32E−02
1	1.96E−03	1.96E−03	1.96E−03	1.96E−03	1.96E−03	1.96E−03	1.96E−03
1.5	2.30E−06	2.30E−06	2.30E−06	2.30E−06	2.30E−06	2.30E−06	2.30E−06
2	2.30E−06	2.30E−06	2.30E−06	2.30E−06	2.30E−06	2.30E−06	2.30E−06
2.5	2.30E−06	2.30E−06	2.30E−06	2.30E−06	2.30E−06	2.30E−06	2.30E−06
3	2.30E−06	2.30E−06	2.30E−06	2.30E−06	2.30E−06	2.30E−06	2.30E−06
Totals	**5.89E−03**	**2.59E−02**	**5.01E−02**	**5.32E−02**	**5.32E−02**	**5.01E−02**	**4.56E−02**

Continued

Depth (cm)	Jun.	Jul.	Aug.	Sept.	Oct.	Nov.	Dec.
0	2.62E−02	2.62E−02	2.30E−02	2.30E−02	2.30E−02	1.77E−02	1.77E−02
0.5	1.32E−02	1.11E−02	1.11E−02	1.11E−02	1.11E−02	1.02E−02	1.02E−02
1	1.96E−03	1.96E−03	1.96E−03	1.96E−03	1.96E−03	1.96E−03	1.96E−03
1.5	2.30E−06	2.30E−06	2.30E−06	2.30E−06	2.30E−06	2.30E−06	2.30E−06
2	2.30E−06	2.30E−06	2.30E−06	2.30E−06	2.30E−06	2.30E−06	2.30E−06
2.5	2.30E−06	2.30E−06	2.30E−06	2.30E−06	2.30E−06	2.30E−06	2.30E−06
3	2.30E−06	2.30E−06	2.30E−06	2.30E−06	2.30E−06	2.30E−06	2.30E−06
Totals	**4.14E−02**	**3.93E−02**	**3.61E−02**	**3.61E−02**	**3.61E−02**	**2.99E−02**	**2.99E−02**

Figure 8 shows the evolution of the shrinkage-swelling of crumb marl as a function of the variation in suction.

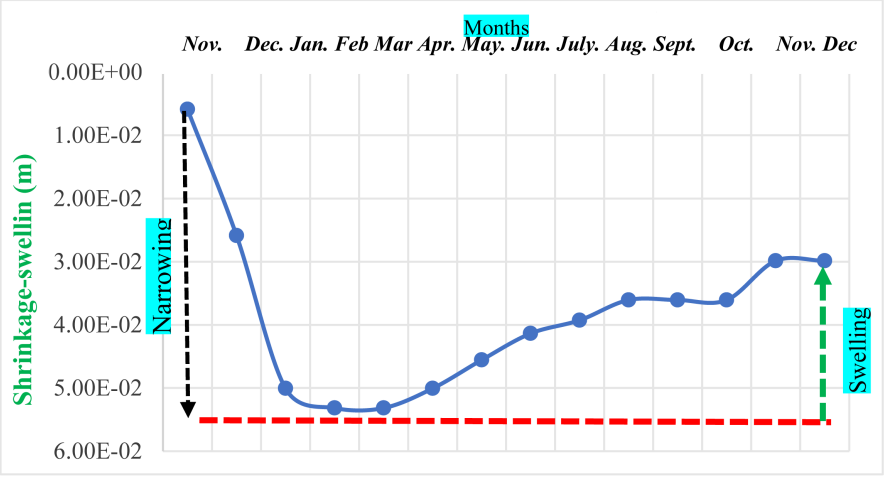

Figure 8. Shrinkage-swell curve of the crumbly marl.

The study of the movement curve shows that the crumb marl is in continuous movement over time. The shape of this curve shows the existence of a shrinkage phase and a swelling phase. The shrinkage phase begins in November and continues until March while swelling takes place during the other remaining months.

In this specific case, if we consider the month of November 2019 as the initial state, the curve is characterized by a sequence of shrinkage and a sequence of swelling and during this period, the vertical movement of the ground is marked by a total contraction of the order of 0.047 m and a swelling of 0.0233 m. The comparison we made shows that more than half of the ground movements are recorded at the superficial part. For example, if we take the example of the month of February, the total displacement of the marl is estimated at 5.32×10^{-2} m and that of the surface is 3.58×10^{-2} m or 67% of the total movement of the ground.

This percentage is explained by the fact that the suction variations are greater at the surface of the ground and that the deeper we go, the more the suction decreases until it reaches more or less constant values.

Figure 9 illustrates the vertical movements of the ground according to climate variation and depth for December 2019, February 2020, November 2020, August 2020, and May 2020.

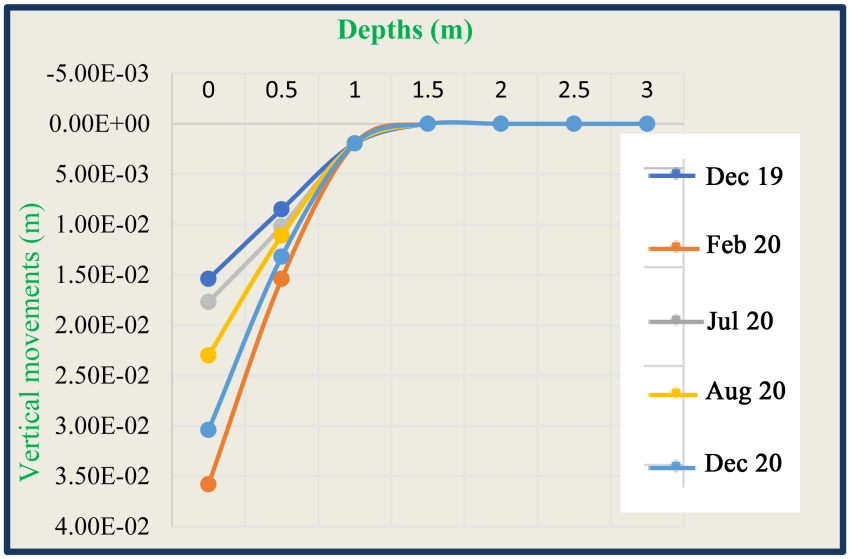

Figure 9. Variation of the volumetric changes of crumbly marl according to the evolution of suction with depth.

We note that ground movements are more accentuated at the upper parts of the layer as we wrote previously. The shrinkage-swellings are intense in the superficial parts then gradually decrease going deeper. For swelling phenomena, the contents are greater in the higher levels which justifies the higher swellings at this level. In the lower parts, under the effect of infiltration, the water can reach certain levels but with low contents. In fact, these water contents fluctuate slightly at depth, leading to more or less stable volume changes in the soil layer. In the same way, the contraction of the soil is synonymous with an increase in suction which is greater in the upper parts of the marl layer and weaker in the lower levels. In this specific case, the swelling is therefore a recovery of the thickness of the layer already lost during contraction, which is why in countries like Senegal where the dry season is longer around nine months out of twelve, the contraction phenomenon must be studied more rigorously before the implementation of construction projects. These two parameters, namely water content and suction, are controlled on the one hand by climatic data which are more reactive in the superficial parts and on the other hand by the characteristics of the soil in question without also forgetting the time parameter.

In addition to determining the amplitudes of vertical movements of the ground over a period of fourteen months, the model also gives us an idea of the depth of the active zone which extends up to 1.25 m from the surface (see Figure 9). In the

following lines, we will carry out this same study on foliated marl with attapulgite and sandy clay with calcareous concretion.

3.2. Modeling the Shrinkage-Swelling of Laminated Marl

Like crumb marl, we will proceed in the same way to model a layer of foliated attapulgite marl with a thickness of three meters. The geotechnical characteristics of the laminated marl are shown in Table 6.

Table 6. Characteristics of the layered marl.

Modulus of elasticity E kPa	Natural water content %	Saturated water content %	Void indive e_0	Porosity n	Permeability k (m/s)	Thermal conductivity (W/m/K)
21232.156	7.6	59.8	1.008	0.50	1.53E−09	50

The vertical displacement values after calculation are grouped in Table 7:

Table 7. Vertical displacement as a function of depth.

Depth (m)	Nov.	Dec.	Jan.	Feb.	March	Apr.	May
0	8.01E−04	5.50E−03	1.40E−02	1.40E−02	1.40E−02	1.40E−02	1.40E−02
0.5	8.01E−04	4.50E−03	5.50E−03	5.50E−03	5.50E−03	5.50E−03	5.30E−03
1	9.54E−07	8.01E−04	8.01E−04	8.01E−04	8.01E−04	8.01E−04	8.01E−04
1.5	9.54E−07	9.54E−07	9.54E−07	9.54E−07	9.54E−07	9.54E−07	9.54E−07
2	9.54E−07	9.54E−07	9.54E−07	9.54E−07	9.54E−07	9.54E−07	9.54E−07
2.5	9.54E−07	9.54E−07	9.54E−07	9.54E−07	9.54E−07	9.54E−07	9.54E−07
3	9.54E−07	9.54E−07	9.54E−07	9.54E−07	9.54E−07	9.54E−07	9.54E−07
Totals	**1.61E−03**	**1.08E−02**	**2.03E−02**	**2.03E−02**	**2.03E−02**	**2.03E−02**	**2.01E−02**
Depth (m)	**Jun.**	**Jul.**	**Aug.**	**Sept.**	**Oct.**	**Nov.**	**Dec.**
0	1.40E−02	1.40E−02	9.50E−03	9.50E−03	8.90E−03	8.90E−03	9.50E−03
0.5	5.30E−03	4.99E−03	4.99E−03	4.99E−03	4.20E−03	4.20E−03	4.20E−03
1	9.54E−08	9.54E−08	9.54E−08	9.54E−08	9.54E−08	9.54E−08	9.54E−08
1.5	9.54E−07	9.54E−07	9.54E−07	9.54E−07	9.54E−07	9.54E−07	9.54E−07
2	9.54E−07	9.54E−07	9.54E−07	9.54E−07	9.54E−07	9.54E−07	9.54E−07
2.5	9.54E−07	9.54E−07	9.54E−07	9.54E−07	9.54E−07	9.54E−07	9.54E−07
3	9.54E−07	9.54E−07	9.54E−07	9.54E−07	9.54E−07	9.54E−07	9.54E−07
Totals	**1.93E−02**	**1.90E−02**	**1.45E−02**	**1.45E−02**	**1.31E−02**	**1.31E−02**	**1.37E−02**

The evolution of shrinkage-swelling phenomena during these fourteen months is shown in Figure 10.

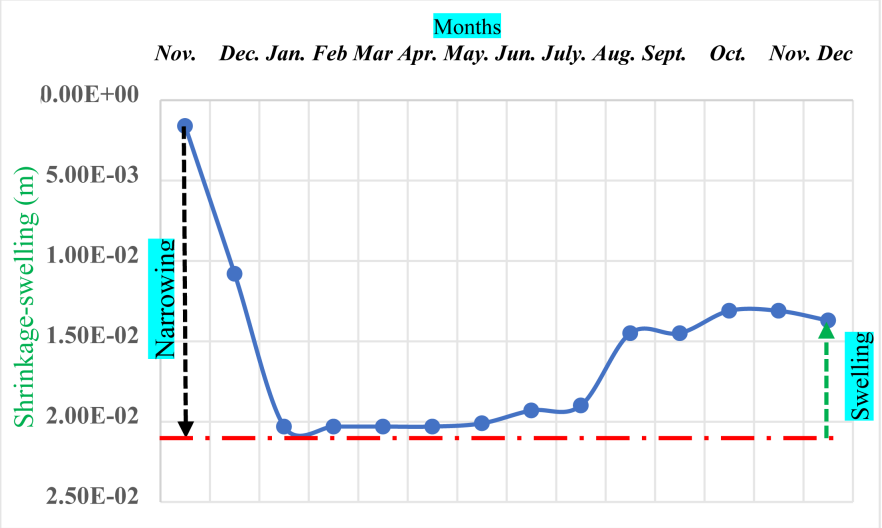

Figure 10. Curve of vertical displacements.

This curve shows an intense contraction in the first three months followed by a more or less stable movement from February until May and once in June, the swelling begins to gain momentum before falling again in the month of December.

Figure 11 allows you to visualize the shrinkage-swelling phenomena as a function of the depth of a few months (December 2019, February 2020, July 2020, August 2020 and December 2020).

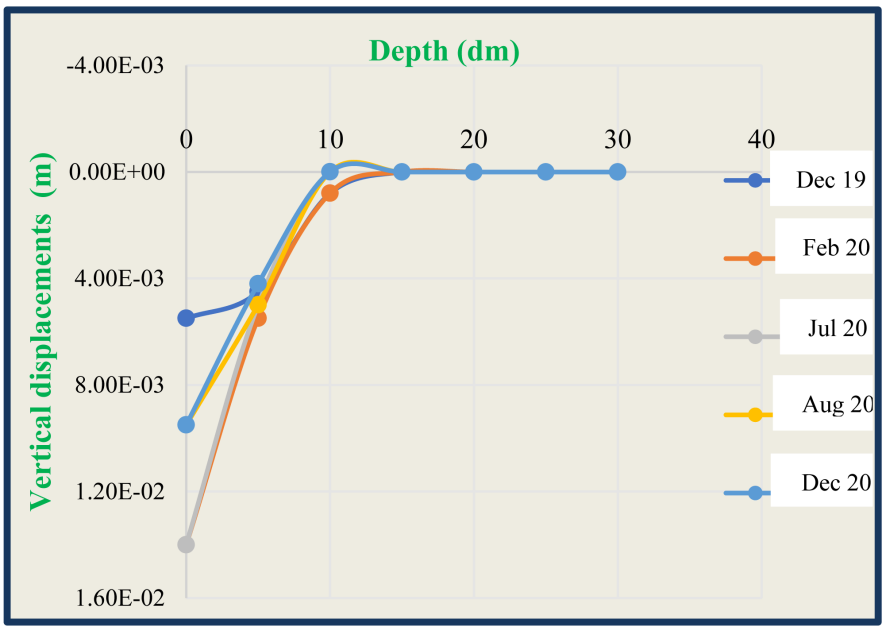

Figure 11. Variation of volumetric changes of the laminated marl according to the evolution of suction with depth.

Unlike the crumb marl, the active zone of foliated marl is located at a depth of 1.5 m and the movements are more accentuated in the upper parts.

3.3. Modeling of the Shrinkage-Swelling of Blackish Sandy Clay

As in the two previous cases, we will model the shrinkage-swelling of sandy clay with limestone concretion with a thickness of 3 m. The characteristics of the clay are shown in Table 8.

Table 8. Some characteristics of blackish sandy clay.

Modulus of elasticity E kPa	Natural water content %	Saturated water content %	Void indive e_0	Porosity n	Permeability k (m/s)	Thermal conductivity (W/m/K)
9079.54	6.7	20.1	0.27	0.21	8.90E−10	2900

After carrying out the different calculation steps, the vertical movements found are grouped together in Table 9.

Table 9. Vertical displacements as a function of depth.

Depth (cm)	Nov.	Dec.	Jan.	Feb.	March	Apr.	May
0	4.20E−03	5.40E−03	2.20E−02	3.40E−02	3.40E−02	3.40E−02	2.90E−02
5	4.20E−03	4.20E−03	1.07E−02	1.60E−02	1.60E−02	1.60E−02	1.07E−02
10	2.23E−06	4.20E−03	4.20E−03	4.20E−03	4.20E−03	4.20E−03	4.20E−03
15	2.23E−06	2.23E−06	2.23E−06	2.23E−06	2.23E−06	2.23E−06	2.23E−06
20	2.23E−06	2.23E−06	2.23E−06	2.23E−06	2.23E−06	2.23E−06	2.23E−06
25	2.23E−06	2.23E−06	2.23E−06	2.23E−06	2.23E−06	2.23E−06	2.23E−06
30	2.23E−06	2.23E−06	2.23E−06	2.23E−06	2.23E−06	2.23E−06	2.23E−06
Totals	8.41E−03	1.38E−02	3.69E−02	5.42E−02	5.42E−02	5.42E−02	4.39E−02
Depth (cm)	**Jun.**	**Jul.**	**Aug.**	**Sept.**	**Oct.**	**Nov.**	**Dec.**
0	2.90E−02	2.90E−02	2.20E−02	2.20E−02	2.20E−02	2.20E−02	2.20E−02
5	1.07E−02	1.07E−02	1.07E−02	1.07E−02	1.07E−02	1.07E−02	1.07E−02
10	4.20E−03	4.20E−03	4.20E−03	4.20E−03	4.20E−03	4.20E−03	4.20E−03
15	2.23E−06	2.23E−06	2.23E−06	2.23E−06	2.23E−06	2.23E−06	2.23E−06
20	2.23E−06	2.23E−06	2.23E−06	2.23E−06	2.23E−06	2.23E−06	2.23E−06
25	2.23E−06	2.23E−06	2.23E−06	2.23E−06	2.23E−06	2.23E−06	2.23E−06
30	2.23E−06	2.23E−06	2.23E−06	2.23E−06	2.23E−06	2.23E−06	2.23E−06
Totals	**4.39E−02**	**4.39E−02**	**3.69E−02**	**3.69E−02**	**3.69E−02**	**3.69E−02**	**3.69E−02**

Figure 12 shows us the evolution of the vertical movements of the sandy clay over time.

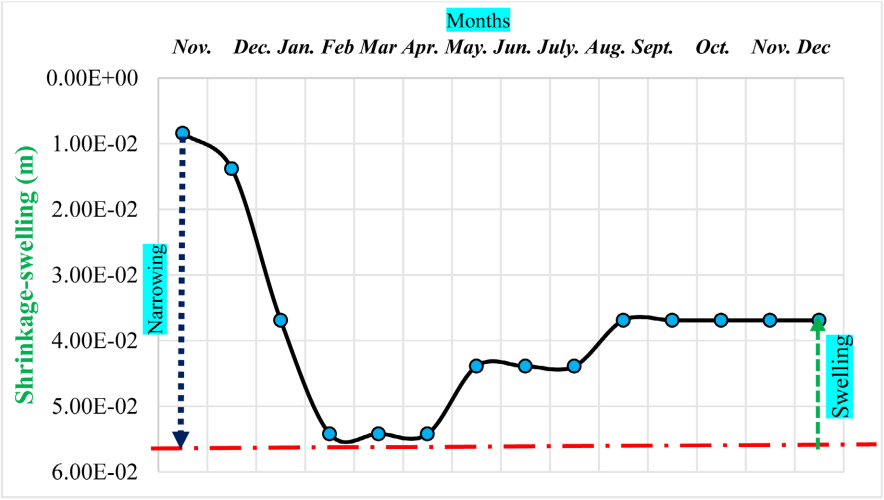

Figure 12. Shrinkage-swelling curve of the blackish sandy clay.

The study of the movement of sandy clay as a function of depth shows a significant contraction in the superficial parts which gradually decreases going deeper before reaching a stable value. The values in Table 9 reveal that the active zone of the sandy clay is located at a depth of 1.5 m. Under the effect of solar radiation and evaporation, water contents gradually decrease at depth. This drop in water content implies an increase in suction depending on the depth and consequently, the movements will be more accentuated in the superficial parts. Subsequently, the month of April marks the end of the contraction and once in May the evolution of swelling becomes rapid then remains constant between May, June and July before beginning another sequence of swelling between August, September, October, November and December. During this period, under the effect of rainfall and infiltration, suction decreases considerably. Once the volume variations of these three soils have been studied, we will proceed in the following lines to make a comparison of these vertical movements over time.

4. Comparison of the Shrinkage-Swelling Curves of These Three Soil Types

The displacement curves of these three types of soil are grouped together in Figure 13, which allows us to make a comparison of shrinkage-swelling during this period.

These curves reveal that crumb marl and sandy clay have similar values, unlike those of laminated attapulgite marl. We note that crumb marl and sandy clay are more affected by shrinkage phenomena with a maximum of 5.42 cm for sandy clay and 5.32 cm for crumb marl. These two soils have the greatest volume changes, unlike the laminated attapulgite marl, the latter of which presents a greater swelling. These values support the results already found in oedometric tests which showed that foliated marl is more swelling followed by crumb marl and lastly sandy clay

with calcareous concretion. During this period, during the fourteen months, we observe that the contractions are more important than the swellings.

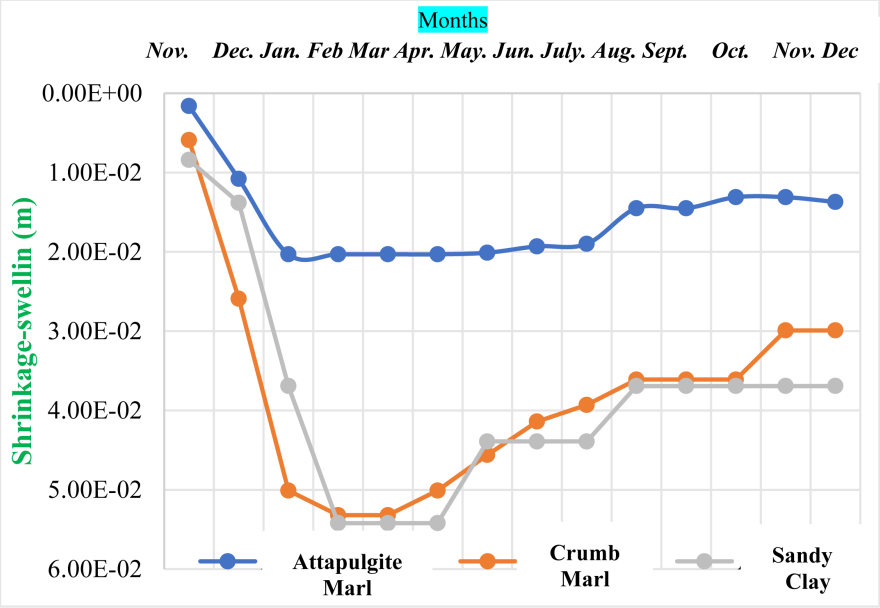

Figure 13. The vertical displacement curves of the three soils.

The significant contraction of crumb marl and sandy clay is explained on the one hand by the fact that their permeabilities are higher than that of laminated marl with respective values of 1.15×10^{-9} m/s, 1.53×10^{-9} m/s and 8.47×10^{-10} m/s. Indeed, a high permeability value promotes rapid evaporation of water and therefore an increase in suction. When the permeability is very low, for example that of laminated marl, this implies slow evaporation, but these conditions favor significant swelling because the pore water will have more time to react with the clay particles. For low permeability values, the fluctuations in water contents are very slow, those which lead to less significant variations in shrinkage-swelling as shown by the movement curve of foliated marl and when the permeability values are high in the case of sandy clay, soil movements are more dynamic with greater shrinkage amplitudes.

In these three examples, the swelling is firstly a recovery of the thickness of the layer already lost during shrinkage. This shows that in countries where the dry season is longer, shrinkage phenomena take place over a long period of time with amplitudes which vary according to climatic data and the intrinsic characteristics of the soil. Among these intrinsic characteristics, we can cite the initial water content, porosity, structure and texture of the soil.

5. Conclusions

The study of volumetric changes in the swelling soils of Diamniadio using the elasticity-based model, which is a predictive model that relies on climate variation to determine vertical soil movements over time. In the proposed approach, the

constitutive relationship for volume change developed by Fredlund and Morgenstern (1976) for unsaturated soils was integrated with the soil-environment model VADOSE/W (GeoSlope). The analysis of the study results on the three soils showed that the model can reproduce vertical soil movements based on climatic data. This method allows for the direct determination of the depth of the active zone of the soil layer, the dynamic area where vertical soil movements occur. The modeling results show that crumbly marl and sandy clay with calcareous concretions are more affected by the re-treatment phenomenon compared to laminated marl. This is explained by the fact that the particle size and permeability of these soils promote greater evaporation. As for swelling, that of the laminated marl is more significant; this more pronounced swelling is consistent with results already found in oedometer tests (Faye *et al*., 2022) [10]. Overall, we can note a good correlation between the vertical movements of the soil and climatic variations.

The maximum shrink-swell movements recorded for these three types of soil can be greater during periods of multiyear drought or in the case of exceptionally wet periods (intense and prolonged rainfall).

From a perspective of model validation based on the elasticity modulus, *in-situ* measurements or a scaled model could be carried out to highlight the results obtained in this study.

Conflicts of Interest

The authors declare no conflicts of interest regarding the publication of this paper.

References

[1] Adem, H.H. and Vanapalli, S.K. (2013) Constitutive Modeling Approach for Estimating *1-D* Heave with Respect to Time for Expansive Soils. *International Journal of Geotechnical Engineering*, **7**, 199-204. https://doi.org/10.1179/1938636213z.00000000024

[2] Fredlund, D.G. and Morgenstern, N.R. (1976) Constitutive Relations for Volume Change in Unsaturated Soils. *Canadian Geotechnical Journal*, **13**, 261-276. https://doi.org/10.1139/t76-029

[3] Briaud, J., Zhang, X. and Moon, S. (2003) Shrink Test-Water Content Method for Shrink and Swell Predictions. *Journal of Geotechnical and Geoenvironmental Engineering*, **129**, 590-600. https://doi.org/10.1061/(asce)1090-0241(2003)129:7(590)

[4] Chao, K.C. (2007) Design Principles for Foundations on Expansive Soils. Ph.D. Thesis, Colorado State University.

[5] Vu, H.Q. and Fredlund, D.G. (2004) The Prediction of One-, Two-, and Three-Dimensional Heave in Expansive Soils. *Canadian Geotechnical Journal*, **41**, 713-737. https://doi.org/10.1139/t04-023

[6] Zhang, X. and Briaud, J. (2010) Coupled Water Content Method for Shrink and Swell Predictions. *International Journal of Pavement Engineering*, **11**, 13-23. https://doi.org/10.1080/10298430802394154

[7] ANACIM (2020) Agence Nationale de l'Aviation Civile et de la Meteorology du Senegal.

[8] Fredlund, D.G. and Rahardjo, H. (1993) Soil Mechanics for Unsaturated Soils. John

Wiley & Sons. https://doi.org/10.1002/9780470172759

[9] Fredlund, D.D., *et al.* (1980) The Prediction of Total Heave. *Proceedings of the* 4*th International Conference on Expansive Soils*, Denver, 16-18 June 1980, 1-17.

[10] Faye, K., Samb, F., Berthaud, Y. and Faye, P.S. (2023) Study and Comparison of Swelling and Compressibility Characteristics of Crumb Marl, Flaky Marl with Attapulgite and Sandy Clay from the Diamniadio Urban Pole at the Oedometer. *Geomaterials*, **13**, 61-70. https://doi.org/10.4236/gm.2023.133005